The 2010 IEEE/RSJ International Conference on
Intelligent Robots and Systems
October 18-22, 2010, Taipei, Taiwan

Material Handling of a Mobile Manipulator Using an Eye-in-Hand Vision System

T. I. James Tsay, *Member, IEEE*, Y. F. Lai and Y. L. Hsiao

***Abstract*—The developed mobile manipulator is primarily composed of a mobile base, a robot manipulator and an eye-in-hand vision system. The material handling of a mobile manipulator has two stages: guiding the mobile base between stations, and picking up a workpiece from a station. Fast landmark recognition and obstacle detection based on color segmentation are proposed for path following, obstacle avoidance and mobile base positioning. Using the machine vision, a vision-based vector field histogram method is modified and applied to guide the mobile manipulator for obstacle avoidance. However, after the mobile manipulator arrives at the station, positioning errors of the mobile base and the non-horizontality of ground inevitably cause position and orientation errors of the mobile base relative to the station. A vision-guided control strategy with a behavior-based look-and-move structure is presented. This strategy is based on six predefined image features. In the designed neural fuzzy controllers, each image feature is taken to generate intuitively one degree of freedom motion command relative to the camera coordinate frame using fuzzy rules, which define a specific visual behavior. These behaviors are then combined and executed in turns to perform grasping tasks.**

I. Introduction

In a semiconductor factory, production lines typically have a small production volume and period, leading to frequent factory re-layouts. Thus, applying mobile manipulators in the production lines of a semiconductor factory is favorable. This study adopts an eye-in-hand vision system to provide visual information not only for the guidance of the mobile base from one station to another, but also for the guidance of the robot manipulator mounted on the mobile base to perform the following pick-and-place operation.

Obstacle avoidance is a necessary capability of an autonomous mobile manipulator. Borenstein and Koren [3] presented and analyzed a modified implementation, called the virtual force field (VFF) method, based on the potential field method (PFM) [5] in 1989. A disadvantage of the method is that doorways are difficult to pass due to repulsive forces. Borenstein and Koren developed an enhanced VFF-based method called vector field histogram (VFH) method in 1991 [2]. VFH steers a fast-moving mobile robot toward the target while avoiding unknown obstacles. Therefore, this study considers VFH as more appropriate than VFF and PFM for fast obstacle avoidance, and proposes a vision-based VFH method.

Beyond the conventional visual servo control methods, behavior-based methods for visual servo control have already been developed in the literature [1][8]. A behavior-based system has been proposed to perform grasping tasks in an unstructured environment, in cases in which the position of the targets is not already known [8]. The controller maps input from the image space to the control values defined in the camera space. The control values are then transformed to joint controls by a Jacobain transformation, revealing that either a hand-eye calibration process has been implemented or the hand-eye relationship is known beforehand.

In the visual guidance of the mobile base, the monocular distance perception is formulated from the perspective projection camera model rather than interpolation of the angle of view (AOV). The VFH algorithm for obstacle avoidance is modified here to consider the surrounding information fed from a monocular camera, improving the noisy binary result using a double-threshold comparator. In the visual guidance of the robot manipulator, the vision system compensates for the uncertainties in location associated with a mobile base or the object. A behavior-based look-and-move control strategy [7] is presented to guide the manipulator to approach the object and accurately position its end-effector in the desired pose.

II. Constructed Mobile Manipulator

A mobile manipulator, as depicted in Fig. 1, was constructed in the Robotic Systems and Control Lab., National Cheng Kung University. It consists mainly of a mobile base, a robot manipulator, and a vision system. The mobile base is balanced using four passive caster wheels at the four corners of the base. It is driven by two powered wheels that provide motion and steering. Steering is accomplished by differential velocity control of the powered wheels. The robot manipulator used here is a vertical articulated manipulator with six degrees of freedom (DOF). The vision system includes one frame grabber and one CCD camera, which incorporates a 10× optical zoom lens with auto focus, allowing the camera to zoom in on distant subjects. The camera is attached to the end-effector of the robot manipulator. The electric power system of the mobile manipulator consists of one UPS and two sealed lead acid

Manuscript received March 12, 2010. This work was supported in part by the National Science Council of the Republic of China under Grant NSC 91-2212-E-006-144.

T. I. James Tsay is with the Department of Mechanical Engineering, National Cheng Kung University, Tainan, Taiwan 70101, R.O.C. (phone: +886-6-275-7575 Ext. 62175; fax: +886-6-237-3726; e-mail: tijtsay@mail.ncku.edu.tw).

Y. F. Lai and Y. L. Hsiao are in the Army, R.O.C..

batteries.

Fig. 1. Developed mobile manipulator.

III. Visual Guidance of the Mobile Base

The visual guidance system of the mobile base is composed of a path following module, an obstacle avoidance module and a positioning module, and switches between the three modules based on the surrounding environment conditions. The path-following module guides the mobile base to travel from one station to another by steering along the predetermined path. Then, the positioning module accurately drives the robot to dock with the station. The aim of obstacle avoidance is to enable a mobile manipulator to work in an object-scattered environment without damaging itself or any of the obstacles it encounters.

A. Landmark Detection and Obstacle Detection

Two orange patterns, one ring and one strip in shape, were used as landmarks for the path following and positioning of the mobile base. The principal axis of a strip-mark indicates the orientation of the mobile base traveling path or that of the mobile base positiong, and the center of gravity (CoG) of a ring-mark locates the site for the arrival mobile manipulator.

The captured image in the RGB color space is first preprocessed using the weighted average filter and converted to HSI color space. In the landmark detection scheme, the preprocessed image is then segmented according to the HSI values of each pixel using image thresholding on the hue and saturation bands. The potential region is formed by the intersection of the binary hue band with the binary saturation band, and followed by the morphological opening and closing operations to suppress noise without significantly affecting the result image. To identify connected regions of pixels within the resulting binary image, the region-based segmentation is achieved through 8-neighborhood labeling. Then, features of the connected pixels can be determined to recognize landmarks. Blob geometry features include roundness and number of holes for ring-mark recognition, and the aspect ratio for strip-mark recognition. Available measurements for landmark recognition include the roundness, the number of holes and the aspect ratio.

In the obstacle detection scheme, a pixel is classified as representing an obstacle or the ground based on color information. The background model is represented in a histogram to present the distribution details of the entire frame traded at each bin. The bins in the histogram are addressed based on the H, S and I values of a color pixel. The background pixel is modeled by a Gaussian distribution, characterized by its mean and standard deviation. Background segmentation is a commonly applied technique to identify foreground elements quickly. Whether a pixel represents the background or an occluding element depends on its intensity and chromaticity. The appearance-based segmentation algorithm should consider the case of achromaticity. The procedure starts by evaluating the saturation of each pixel. A pixel is assumed to have a valid chromaticity only if the saturation is above a given threshold. The background is segmented from the result of binary hue, saturation and intensity image by logical multiplication (AND operation). The output is a binary mask marking pixels interpreted as the background.

B. Monocular Distance Perception

Cheng [4] and Taylor [6] proposed an analysis for the monocular camera that was tilted such that the entire field of view (FOV) of the camera intersected the floor. A linear division of the AOV was used to interpolate the viewing angle between camera's principal axis and the ray of light traced from lens center to the object on the ground. Since the accuracy deteriorates as the AOV increase, this study derives the monocular distance perception from the perspective projection model rather than interpolation of AOV.

The side view of the camera imaging model using perspective projection geometry, is illustrated in Fig. 2. The camera angle, θ_{cp}, is measured from vertical to the principal axis. The vertical viewing angle, θ_v, and the longitudinal distance relative to the object on the floor, Y, can be calculated with trigonometry.

$$\theta_v = \tan^{-1}(\tan(\theta_y/2)\cdot(\frac{2v'}{H_{img}}-1)) \quad (1)$$

$$Y = E\cdot\tan(\theta_{cp}-\theta_v) \quad (2)$$

where θ_y is the vertical AOV of the camera, v' denotes the vertical length from the object point to the principal point in pixels, H_{img} represents the number of pixels per column on CCD, and E is the elevation of the camera above the floor. The lateral distance relative to the object can also be derived with trigonometry. The horizontal viewing angle, θ_u, the length from the lens center to the camera principal point projected on the floor, L, and the lateral distance relative to the object on the floor, X, can be computed as follows.

$$\theta_u = \tan^{-1}\left(\tan\frac{\theta_x}{2}(\frac{2u'}{W_{img}}-1)\right) \text{ and } L = \frac{E}{\cos\theta_{cp}} \quad (3)$$

$$X = L\cdot\tan\theta_u \quad (4)$$

where θ_x is the horizontal AOV of the camera, u' denotes the horizontal length from the object point to the PP in pixels, and W_{img} represents the number of pixels per row on CCD.

To determine the orientation of the strip-mark on the floor with respect to the mobile base frame, an image point moving along the principal axis with a small offset from the mark's CoG is selected first. After transforming both the mark's CoG

and this selected point from the image plane to the mobile base frame, two points in the mobile base frame are obtained. Consequently, the orientation of the strip-mark in the mobile base frame can be achieved.

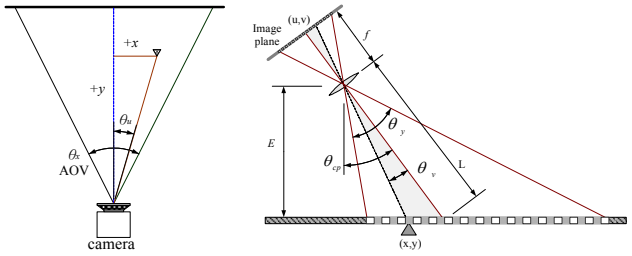

(a) Top view (b) Side view

Fig. 2. Perspective projection of a point (x,y) onto a point (u,v).

C. Path Following

Path following is intended to steer the mobile manipulator along a predefined path, and eradicates both the orientation and lateral errors. The path following error of the mobile manipulator is composed of a lateral error, $|d|$, and an orientation error, θ_{err}. The lateral error $|d|$ is defined as the distance from the origin of the mobile base frame to the pre-specified path. While the orientation error, θ_{err}, is defined as the angular deviation of the robot's heading direction from the direction of the desired path, as shown in Fig. 3. Both d and θ_{err} can be determined by (5). When the strip-marks are exploited as a landmark with spacing intervals in the workspace, each mark simply directs a ray as the preferred path for the mobile manipulator to follow. The landmark orientation recorded in the path following module by the mobile manipulator will not be updated until next mark is presented.

$$d = sign(\theta_{lr}) \cdot |\underline{\boldsymbol{l}} \times \boldsymbol{r}| = sign(\theta_{lr}) \cdot |\underline{\boldsymbol{l}}| \cdot |\boldsymbol{r}| \cdot |\sin\theta_{lr}| \text{ and } \theta_{err} = \theta - \theta_l \quad (5)$$

where the unit vector $\underline{\boldsymbol{l}}$=(cos$\theta_l$,sin$\theta_l$) denotes the orientation of the strip-mark on the floor in θ_l with respect to x-axis of the world frame.

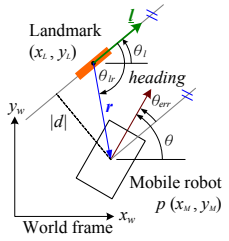

Fig. 3. Path following coordinates.

Considering the smooth steering and the path error convergence for the mobile manipulator, the steering angle is determined from the lateral error, d, and the angular error, θ_{err}. A monotonic increasing function, Gamma-function with saturation, is introduced to the steering angle control.

$$\theta_{steer} = -\theta_{err} - sign(d) \cdot \theta_{steerMax} \cdot \left(\frac{d}{d_{\max}}\right)^{\gamma} \quad \text{for } |d| < d_{\max} \quad (6)$$

$$\theta_{steer} = -\theta_{err} - sign(d) \cdot \theta_{steerMax} \quad \text{otherwise}$$

where $d_{\max}$ and $\theta_{steerMax}$ are the threshold values of the lateral error and steering angle, respectively. A large heading velocity together with a large angular velocity severely damages the stability and safety of the mobile manipulator. Therefore, the heading velocity, V, is calculated as follows.

$$V = (V_{\max} - V_{\min}) \cdot \left(1 - \left|\frac{\theta_{steer}}{\theta_{steerMax}}\right|\right)^{\gamma} + V_{\min} \quad \text{for } |\theta_{steer}| < \theta_{steerMax} \quad (7)$$

$$V = V_{\min} \quad \text{otherwise}$$

where $V_{\max}$ denotes the maximum heading velocity depending on the visual depth and the image sampling rate. To prevent V from falling to zero, a minimum heading velocity is set as $V_{\min}$.

D. Obstacle Avoidance

The visual guidance system of the mobile base should switch the controller from the path following module to the obstacle avoidance module when the obstacle is encountered. The robot is aware of the desired travel path, but has to plan a path around obstacles. A vision-based VFH method is proposed in this study.

After the vision-based mobile manipulator senses the surrounding environment with the camera and segments obstacles from background, the distribution of obstacles on the image plane, called the obstacle distance histogram (ODH), is then constructed from the obstacle edges. Next, the ODH is transformed from the image plane to Cartesian mobile base frame by the coordinate transformation. A drawback of VFH is that it treats the mobile manipulator as point-like vehicle. By contrast, the proposed method compensates for the width of the robot with an obstacle enlargement process. The enlargement is performed by eroding the obstacle-free space in the grayscale ODH, with one-half the width of the mobile manipulator on both the left and right hand sides of each obstacle on the ODH. Then, the ODH in the Cartesian mobile base frame is mapped onto the polar mobile base frame to build the polar obstacle histogram (POH). The direction of the POH is set by the direction from the obstacles to the robot center point, and the magnitude of the POH is the distance from the origin of the mobile base frame to the obstacles. A POH results are plotted in Fig. 4.

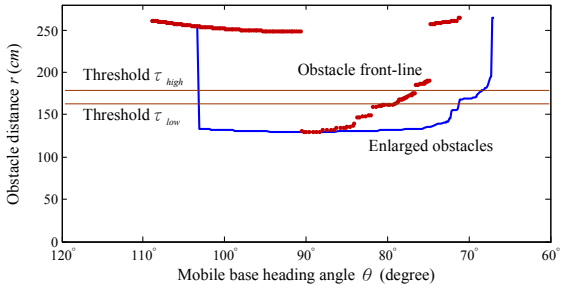

Fig. 4. Polar obstacle histogram.

Once the polar histogram is obtained, VFH determines the open intervals (i.e., the obstacle-free sectors) based on the binary polar histogram using one fixed threshold. This approach may cause a problem in environments with several narrow openings, since the corresponding opening in the histogram frequently oscillates between an open and a blocked state in a short time. In such a situation, the robot's

heading can switch several times between the narrow opening and another opening, leading to indecisive behavior when the mobile manipulator comes very close to an obstacle. The proposed method solves this problem by introducing the Schmitt trigger as a comparator with the hysteresis band through the overlapping ranges. This double threshold comparator is widely utilized for waveform shaping under noisy conditions. The Schmitt trigger does not switch when the input is within the noise-rejection range, but does switch when the input is over τ_{high} or under τ_{low}.

Given the mobile manipulator maximum velocity, V_{max}, and the robot deceleration, a, the necessary time and distance, τ, to stop the robot before collision can be computed based on the accelerated movement formula.

$$\begin{cases} h_i = 1 \text{ (open)} & \text{if } h_i > \tau_{high} \\ h_i = 0 \text{ (block)} & \text{if } h_i < \tau_{low} \\ h_i = h_{i-1} & otherwise \end{cases} \quad (8)$$

In the above equations, h_i denotes the i^{th} bin value of the polar histogram, and τ_{high} or τ_{low} represents the higher or lower trigger threshold which equals τ plus or minus half the noise rejection range.

In the second data reduction stage, the same concept of steering selection in original VFH is applied. All of the opening sectors in the binary POH have been found, and the best direction of travel must be based on the direction to the desired path. The nearest open sector is chosen as the direction of travel until the next update cycle. Once no obstacles are perceived, the mobile manipulator turns to follow the strategic direction to return to the path center. The mobile manipulator runs initially at its maximum speed, and attempts to maintain this speed unless obstacles push its speed down. Since the velocity control utilizes the same algorithm as that described in the previous subsection, the bulk of the method is not repeated here.

Due to the nonholonomic constraint of the differential drive architecture, our mobile manipulator cannot move sideways. The path tracking algorithm must be able to generate a smooth and continuous trajectory with the specific direction of the tangent at each waypoint. Considering the continuity, convex hull property and affine invariance, the Bezier curve is appropriate for this task and is applied herein to generate a trajectory for the robot to detour obstacles.

E. Positioning

The schematic layout of the station is shown in Fig. 5. A positioning mark for the position control consists of a ring and a strip mark. The ring mark's CoG is set in front of the desired robot location at a certain distance. The principal axis of the strip mark is set to pass through the centerline of the mobile base in the desired location and parallel to the station. Once the mobile manipulator closes to the station and the positioning mark is identified by the eye-in-hand camera. The positioning module tends to drive the mobile base toward the desired location and align the mobile base centrally along the strip mark's principal axis.

Once the mobile manipulator arrives at the station labeled by a positioning mark, it performs an evaluation to double-check whether the robot lateral location error stays within the acceptable range. If it does not, then the mobile manipulator departures to move backward a while and repeats the above procedure one more time. To align the mobile base with the station, the robot manipulator moves the eye-in-hand camera from the mobile base heading position to the right side position, where the camera looks straight down at the docking-mark. To enhance the visual measurement accuracy during docking, the optical lens can be zoomed in to fill the whole docking-mark in the camera's FOV. The accurate alignment is further divided into two substages. First, the angular positioning error of the mobile base is adjusted, then the longitudinal error is eliminated.

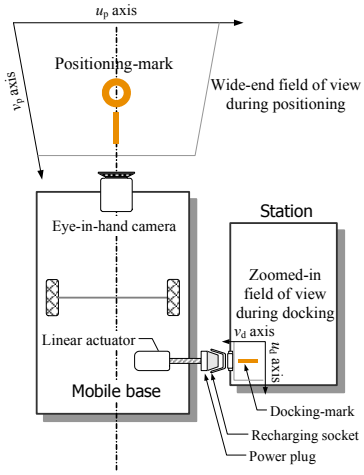

Fig. 5. Station layout.

IV. Visual Guidance of the Robot Manipulator

Fig. 6 shows the behavior-based look-and-move control structure [7]. For the reference features, the end-effector is initially driven by a teaching box to a location that allows the gripper to grasp the workpiece. Then, the end-effector is driven to the "target location", which is a safe distance from the preceding location (in this case, 10 cm above it). The reference features correspond to the image at the target location. In this study, the workpiece to be picked up by the manipulator's end-effector is a rectangular parallelepiped. The images of the workpiece are captured from above by the eye-in-hand camera, as the end-effector moves toward the workpiece. The image of the workpiece's top surface is a quadrangle. Only information about the quadrangle is of interest, so the captured image is firstly preprocessed to obtain a clear image of the quadrangle, from which six predefined image features can be calculated. The six image features include two coordinates of the CoG, relative distance, two ratios of lengths of two opposite sides and the principal angle of the quadrangle in the image plane. Then, six designed neural fuzzy controllers map image feature errors in the image space onto motion commands in the camera space. Also, each mapping from image space to camera's Catesian space is mediated by fuzzy rules, and defines a particular

vision-based behavior.

The complete manipulation task involved in implementing a human-like visual servoing method is first divided into two complex vision-based behaviors, "Approach" and "Surround", and one basic operation, "Catch". The Approach behavior is the translational motion of the camera toward the workpiece, which is further divided into two basic behaviors – "Center" and "Zoom". The Center behavior is based on the first two image features, two coordinates of the CoG of the quadrangular image; this behavior translates the camera along the ${}^{C}X$ and ${}^{C}Y$ axes of the camera frame to keep the CoG of the quadrangular image at the desired pixel in the image plane. However, the Zoom behavior is based on the relative distance of the quadrangular image; it moves the camera along the ${}^{C}Z$ axis of the camera frame to keep the size of the object as a predefined value. Additionally, the Surround behavior is the orientational motion of the camera to keep the workpiece in the gripper, and is further divided into three basic behaviors - Yaw, Pitch and Roll. The Yaw and Pitch behaviors are based on two ratios of lengths of two opposite sides of the quadrangular image; they rotate the camera to adjust its orientation. Moreover, the Roll behavior is based on the principal angle of the quadrangular image; it rotates the camera about ${}^{C}Z$ so that the principal angle equals that in the reference image, in which the gripper's two fingers are arranged parallel to the short sides of target. Fig. 7 depicts these vision-based behaviors. Furthermore, the Catch is a non vision-based operation.

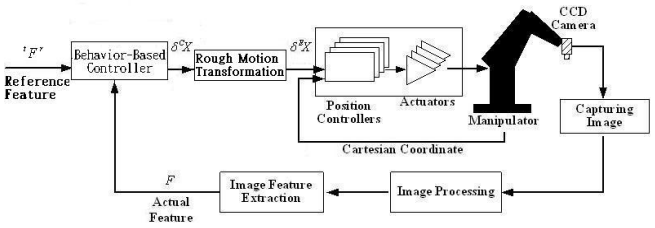

Fig. 6. Behavior-based look-and-move control structure.

Six simple neural fuzzy controllers employing back-propagation are designed herein. One image feature error is input to each controller, which changes one D.O.F. of the camera motion as the output. The back-propagation algorithm is used only to adjust the consequents of fuzzy rules for each neural fuzzy controller at each iteration during the manipulation. Restated, the camera is guided intuitively according to the image features on the image plane. Notably, the output values of the neural fuzzy controllers are defined in the camera frame, but the motion commands sent to the manipulator's controller are relative to the end-effector frame. Consequently, the output values of the neural fuzzy controllers cannot be immediately sent to the manipulator's controller. In this study, the pose of the camera in relation to the end-effector is invariant, so the camera and the end-effector can be treated as a rigid body. After the motion of the rigid body has been analyzed, the transformation from the output values in relation to the camera frame to the motion commands with respect to the end-effector frame is obtained. Apparently, this hand-eye configuration is inaccurate. However, the designed neural fuzzy controllers handle the inaccuracy by tuning the consequents of the fuzzy rules according to the back-propagation algorithm. This process saves considerable time without the intensive computation associated with hand-eye calibration.

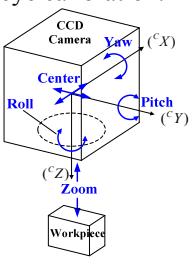

Fig. 7. Motion of defined vision-based behaviors.

V. Experimentation

A. Experimental Setup

The visual guidance used in experiments has two stages: guiding the mobile base to a predefined station and picking up a workpiece from the station. The first stage can further be divided into two substages: navigation and positioning. The camera pose and its zoom position have different settings for both two substages. During the navigation substage, the camera zoomed at the wide-end is raised 178.5cm upward from the floor and pitched 62º downward from the horizontal axis to its optical principal axis. In the positioning substage, the camera zoomed in close-up view is initially raised 140cm upward from the floor and commanded to turn right from look-ahead to vertical downward between the mobile base and the station. In the second stage, the camera is zoomed at the wide-end and the end-effector of the manipulator is firstly driven to the top location, about 40cm above the surface of the station. The workpiece to be picked up is tilted by 6° to the station surface to simulate non-flat ground in the application stage.

B. Experimental Results

Fig. 8 depicts the trajectory and heading angle of the mobile manipulator during obstacle avoidance. Once the first obstacle ($chair_1$) is detected on the image and found to block the desired path at point 1, the mobile manipulator switches to the obstacle avoidance module and deviates from the specified path. The sub-goal (temporary target at point 2) location is first determined with the proposed vision-based VFH method, and a trajectory is generated by path planning based on the Bezier curve. After detouring the obstacle, the second obstacle ($chair_2$) is detected but it does not block its path. Accordingly, the path following module returns the robot to the original assigned path.

The path following module performs the approaching stage of the positioning module. Fig. 9 illustrates the successful positioning trajectory and heading angle of the mobile manipulator during positioning, and the mark locations found on image plane. The mobile manipulator stops behind a positioning mark 60cm from the front edge of mobile

manipulator to the centroid of the ring mark, as shown in Fig. 9(a). To align the robot finely with the station, the robot manipulator is commanded to turn right from look-ahead to vertical downward (interval during 62-78 sec) between the mobile base and the station after the robot arrived at the station. The docking mark does not appear in the image in Fig. 9(b) because of the blurred-motion image during the manipulator movement.

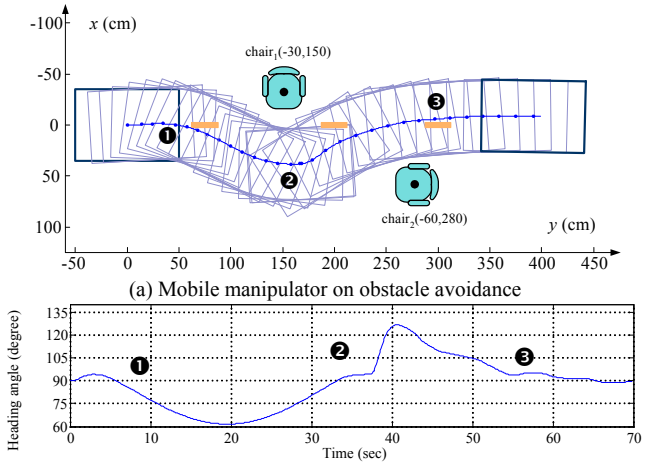

(a) Mobile manipulator on obstacle avoidance

(b) Heading angle of mobile manipulator

Fig. 8. Obstacle avoidance performance of developed mobile manipulator.

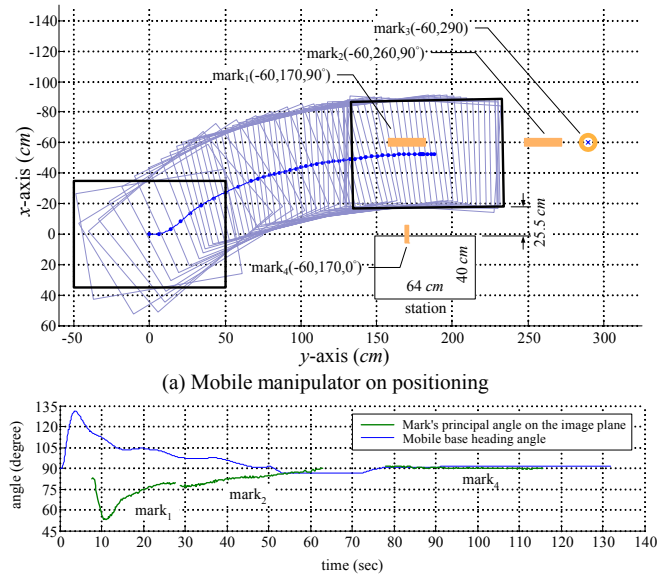

(a) Mobile manipulator on positioning

(b) Mobile base heading angle and mark's principal angle on the image

Fig. 9. Positioning Performance of developed mobile manipulator.

In the experiment performed to evaluate the positioning performance of the eye-in-hand manipulator, the end-effector of the manipulator is firstly driven to the top location. Then, the end-effector is visually guided to grasp the workpiece according to the presented control strategy with the preset parameters. Fig. 10 displays the images in the course of approaching the workpiece.

VI. Conclusion

This work completely constructed an autonomous mobile manipulator for material handling, which mainly consists of a mobile base, a robot manipulator and an eye-in-hand vision system. The vision system provides visual information not only for the guidance of the mobile base from one station to another, but also for the guidance of the robot manipulator mounted on the mobile base to perform the following pick-and-place operation. In the visual guidance of the mobile base, the eye-in-hand CCD camera is used as a ranging sensor. The relative distance is measured with a formalized relationship among the camera elevation, viewing angle and angles of view. Using the machine vision, a vision-based VFH method is proposed to guide the mobile base for obstacle avoidance. Finally, the mobile base docks with the station for the following grasping operations within a permissible level of positioning error. Positioning errors of the mobile base and the non-horizontality of ground inevitably cause position and orientation errors of the mobile base relative to the station. This paper presents a novel behavior-based look-and-move control strategy to guide the manipulator to approach the workpiece and accurately position its end-effector in the desired pose.

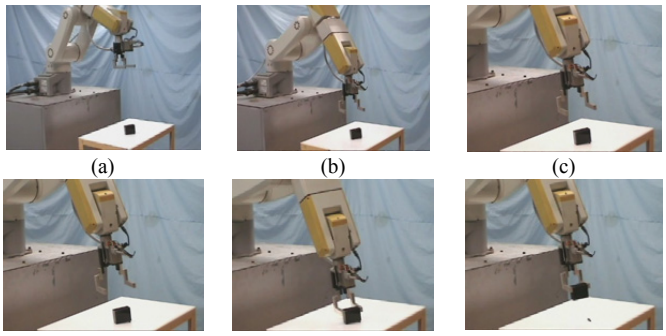

(a) (b) (c)

(d) (e) (f)

Figs. 10(a)~(f) Images in the course of approaching the workpiece, based on the presented control strategy; (a)~(b) approaching stage; (b)~(c) fine positioning stage; (d)~(f) Catch operation.

References

[1] A. Anglani, F. Taurisano, R. De Giuseppe and C. Distante, "Learning to grasp by using visual information," in *Proc. IEEE Int. Symp. Computational Intelligence in Robotics Automation*, Nov. 1999, pp. 7-14.

[2] J. Borenstein and Y. Koren, "The vector field histogram - fast obstacle avoidance for mobile robots," *IEEE Trans. Robot. Automat.*, vol. 7, June 1991, pp. 278-288.

[3] J. Borenstein and Y. Koren, "Real-time obstacle avoidance for fast mobile robots," *IEEE Trans. Syst., Man, Cybern.*, vol. 19, no. 5, Sept./Oct. 1989, pp.1179-1187.

[4] G. Cheng and A. Zelinsky, "Real-Time Visual Behaviours for Navigating a Mobile Robot," in *Proc. IEEE/RSJ Int. Conf. Intelligent Robots Systems*, vol 2, Nov. 1996, pp. 973-980.

[5] O. Khatib, "Real-time obstacle avoidance for manipulators and mobile robots," in *Proc. IEEE Int. Conf. Robotics Automation*, 1985, pp. 500–505.

[6] T. Taylor, S. Geva and W. W. Boles, "Monocular Vision as a Range Sensor," in *Proc. Int. Conf. Computational Intelligence for Modelling, Contr., Automat.*, Aug. 2004, pp. 566-575.

[7] T. I. J. Tsay and Y. F. Lai, "Behavior-based pose control of mobile robots with an uncalibrated eye-in-hand vision system," in *Proc. 36th Int. Symp. Robotics*, Nov. 2005.

[8] Z. Wasik and A. Saffiotti, "A hierarchical behavior-based approach to manipulation tasks," in *Proc. IEEE Int. Conf. Robotics Automation*, Sept. 2003, pp.2780-2785.